

# Revisiting the nuclear magnetic octupole moment

S. Bofos<sup>a,1</sup>, T.J. Mertzimekis<sup>a,\*</sup>

<sup>a</sup>*National and Kapodistrian University of Athens, Zografou Campus, Athens, GR-15784, Greece*

---

## Abstract

The nuclear magnetic octupole moment is revisited as a potentially useful observable for nuclear structure studies. The magnetic octupole moment,  $\Omega$ , is examined in terms of the nuclear collective model including weak and strong coupling. Single-particle formulation is additionally considered in the overall comparison of theoretical predictions with available experimental data. Mirror nuclei symmetry is examined in terms of the magnetic octupole moment isoscalar and isovector terms. A full list of predictions for  $\Omega$  of odd-proton and odd-neutron nuclei in medium-heavy mass regimes of the nuclear chart is produced aiming at providing starting values for future experimental endeavors.

*Keywords:* Nuclear magnetic octupole moment, strong coupling, mirror nuclei

---

arXiv:2406.16429v1 [nucl-th] 24 Jun 2024

---

\*Corresponding author.

*Email address:* [tmertzi@phys.uoa.gr](mailto:tmertzi@phys.uoa.gr) (T.J. Mertzimekis)

<sup>1</sup>Present address: CEA DES/IRENE/DER/SPRC/LEPh, France

## Contents

1. Introduction .....	3
2. Definitions and models .....	3
2.1. Single-Particle Model .....	4
2.2. Collective Model .....	4
2.2.1. Strong coupling case .....	5
2.2.2. Weak coupling case .....	5
3. Comparison with experimental results and predicted values for unmeasured cases .....	6
4. Octupole moments and mirror nuclei .....	9
5. Conclusions .....	10
References .....	11
Explanation of Tables .....	18

## 1. Introduction

The nucleus is conventionally described using a hierarchy of static electromagnetic moments. The most known, magnetic dipole [1, 2] and electric quadrupole [3] moment have been studied extensively and have given much information about nuclear structure, while the next higher, the magnetic octupole moment, remains relatively unexplored. A systematic study of octupole moments will help place constraints on the poorly known isoscalar part of nuclear spin-spin forces [4] and in addition will reduce the uncertainty of nuclear Schiff moments [5]. The main reason for the lack of information about octupole moments is the great difficulty in deducing the magnetic octupole moment,  $\Omega$ , from measurements of the hyperfine intervals, since it requires knowing atomic-structure couplings, that become inaccurate for multivalent atoms. There are only few cases that special features of the nuclei enable us to extract their octupole moment from measurements of hyperfine intervals. As a result, up to now,  $\Omega$  of only 21 isotopes have been measured [6–29]. This lack of experimental results makes the prediction of  $\Omega$  extremely difficult as there is no nuclear model that ensures the appropriate description of  $\Omega$ . The goal of this work is to review the already known information about  $\Omega$  and collect the available experimental data in order to compare them with the predictions of nuclear models attempting to explore any possible trends. This is the first attempt to compare experimental data of  $\Omega$  with the predictions of various nuclear models since the work of Suekane and Yamaguchi in 1957 [30]. In their work, the authors suggested that the strong coupling case of the collective model is the most favorable to describe  $\Omega$  properly.

## 2. Definitions and models

The nuclear magnetic octupole moment ( $\Omega$ ) is defined as  $\Omega = -M_3$ , where  $M_3$  is the expectation value of the corresponding operator [31]

$$M_\lambda^\mu = \mu_N \int \Psi^* \left( \nabla r^\lambda C_\mu^{(\lambda)}(\theta, \phi) \right) \cdot \left( g_l \frac{2}{\lambda+1} \mathbf{L} + g_s \mathbf{S} \right) \Psi dv, \quad (1)$$

where the integral is over the nuclear volume  $v$  and

$$C_\mu^{(\lambda)}(\theta, \phi) = \left( \frac{4\pi}{2\lambda+1} \right)^{1/2} Y_{\lambda\mu}(\theta, \phi).$$

is the multipole tensor operator of order  $\lambda$  with parity  $(-1)^\lambda$ .  $Y_{\lambda\mu}$  denotes the normalized spherical harmonic function of order  $\lambda, \mu$ .

The  $M_3$  operator, given in Eq. 1, differs in nature from the nuclear dipole moment which is a vector. If the wave function for a nucleus with spin  $I$  in the magnetic substate  $m$  is  $\Psi_I^m$ , then the magnetic moment of order  $\lambda$  is the expectation value of the substate with the maximum spin projection

$$M_\lambda = \langle \Psi_I^I | \hat{M}_\lambda | \Psi_I^I \rangle. \quad (2)$$

This quantity vanishes for even  $\lambda$  and  $\lambda > 2I$ . So, it becomes clear that  $\Omega \neq 0$  for values  $I \geq 3/2$  [30]. A non-zero value of  $\Omega$  may be related to the octupole deformation of the nucleus. The study of the octupole deformation and its evolution in nuclei presents great opportunities for both experimental and theoretical research, as it can reveal important issues on symmetries of the nuclear forces (see example works Refs. [32–40]).

The main problem with the calculation of the  $\Omega$  is to find the appropriate wave functions to describe the nucleus. Consequently,  $\Omega$  can be deduced using various models, such as:

- Single-particle model
- Collective model

The relevant expressions for  $\Omega$  based on these nuclear models are deduced below and the corresponding predictions are compared with the experimental data, where available. Besides these models, a mean-field approach in calculating  $\Omega$  could seem a rather straightforward task; however, there is very limited information on such efforts in literature [41], stressing the need for more work along these lines.

### 2.1. Single-Particle Model

In the extreme single-particle model  $\Omega$  is expressed as [31]

$$\begin{aligned} \Omega = & + \mu_N \frac{3}{2} \frac{(2I-1)}{(2I+4)(2I+2)} \langle r^2 \rangle \\ & \times \begin{cases} (I+2)[(I-3/2)g_l + g_s] \text{ for } I = l + \frac{1}{2}, \\ (I-1)[(I+5/2)g_l - g_s] \text{ for } I = l - \frac{1}{2}, \end{cases} \end{aligned} \quad (3)$$

where  $g_l$  and  $g_s$  are constants determined by the type of the valence nucleon. More specifically, their values are

$$\begin{aligned} g_l = 1 \text{ and } g_s = +5.587 \text{ for valence proton,} \\ g_l = 0 \text{ and } g_s = -3.826 \text{ for valence neutron.} \end{aligned}$$

The aforementioned bare nucleon values correspond to the extreme single-particle model. In order to account for observed deviations between experimental values and the predictions of extreme single-particle model, effective  $g$  factors that take into account configuration mixing effects can be adopted. Typical selections of these effective values are  $g_s^{eff} = 0.7g_s$  and  $g_l^{eff} = g_l + \delta g_l$  where  $\delta g_l = +0.1$  for unpaired proton and  $\delta g_l = 0.0$  for unpaired neutron. We will refer to this case as the *effective* single-particle model hereafter.

The extreme single-particle model should not be trusted for more than a rough estimation of the value of  $\Omega$ , as the correct values depend strongly on nuclear many-body effects, more specifically on core polarization mediated by the nucleon spin-spin interaction [4, 42]. This is analogous to the Schmidt limits in magnetic dipole moments [43].

### 2.2. Collective Model

The collective degrees of freedom are associated with deformations in shape with approximate preservation of volume. The normal coordinates of these oscillations would be the expansion parameters  $\alpha_{\lambda\mu}$  of the nuclear surface defined by

$$R(\theta, \phi) = R_0 \left[ 1 + \sum_{\lambda\mu} \alpha_{\lambda\mu} Y_{\lambda\mu}(\theta, \phi) \right], \quad (4)$$

where  $R_0$  is the equilibrium radius. In the basis of the collective model, the magnetic octupole moment operator is considered comprising two separate parts: (a) the core part, which acts on the nucleons that constitute the filled shells, and (b) the particle part, which acts on the particles outside the core. The coupling term of the Hamiltonian that describes the interaction of the angular momentum of the surface with the angular momentum of the particles is given by

$$H_{int} = - \sum_p k(r_p) \sum_{\lambda\mu} \alpha_{\lambda\mu} Y_{\lambda\mu}(\theta_p, \phi_p), \quad (5)$$

where the summation over  $p$  should be considered for the valence nucleons. The term  $k(r_p)$  is related to the strength of the coupling between the angular momenta. The assumption of a sharp nuclear boundary implies that  $k(r_p)$  has the form of a delta function, allowing the use of the constant  $k$  [44]. The strong interaction between the core and the valence nucleons and the interaction of the valence nucleons with themselves are neglected. Two extreme cases are examined in the present work, where the coupling between the core and the particles is either strong or weak.

### 2.2.1. Strong coupling case

The form of the operator that acts on the particles is given by Eq. 1 with the appropriate change in the sign. The action of this operator should be summed over all valence nucleons. As for the operator that acts on the core of the nucleus, starting by the basic Eq. 4 and considering quadrupole deformation of the nucleus ( $\lambda = 2$ ) we get the expression [30]

$$\hat{\Omega}_c = -\frac{i}{28} \frac{3AM}{4\pi\hbar} g_R R_0^4 \sum_{\mu=-2}^{\mu=2} \mu(17 - 5\mu^2) \alpha_{2\mu}^* \dot{\alpha}_{2\mu}, \quad (6)$$

where  $g_R \simeq Z/A$  is the  $g$  factor of the core and  $M$  is the nucleon mass. The choice of  $\lambda = 2$  is not arbitrary, but based on the fact that second-order deformations are considered more impactful on the octupole magnetic moment, in contrast with higher order terms which are often neglected by researchers.

Using the strong coupling wave functions described in Ref. [44] the octupole magnetic moment is obtained as

$$\Omega = P_3(\Omega_{sp} + \Omega_0), \quad (7)$$

where  $P_3$  and  $\Omega_0$  are given by

$$P_3 = \frac{2I(2I-1)(2I-2)}{(2I+2)(2I+3)(2I+4)}, \quad (8)$$

$$\Omega_0 = -\frac{30}{49} \sqrt{\frac{2}{3}} g_R R_0^2, \quad (9)$$

if  $j$  is assumed to be a good quantum number, with  $\Omega_{sp}$  given by Eq. 3.

As a matter of fact, Eq. 8 is correct for  $I > 3/2$ . When  $I = 3/2$  the degeneracy of two states occurs and the wave function becomes complicated. Consequently, for  $I = 3/2$  the octupole moment is expressed as

$$\Omega \simeq \frac{19}{35} \Omega_{sp} + \frac{1}{35} \Omega_0 \quad (10)$$

### 2.2.2. Weak coupling case

For the weak coupling case perturbation theory can be used, considering  $H_{int}$  as a small perturbation. Following the same procedure for the operators as with the strong coupling case results in the expression for the octupole moment correct up to second order in  $H_{int}$  ( $I = j$ )

$$\Omega = \Omega_p + \Omega_c, \quad (11)$$

where

$$\Omega_p = \Omega_{sp} \left[ 1 - k^2 \frac{\hbar\omega}{2C} \sum_{j'} \frac{\langle j|h_2|j'\rangle^2}{(\hbar\omega + \Delta_{jj'})^2} + k^2 \frac{\hbar\omega}{2C} \sum_{j'j''} \frac{\langle j|h_2|j''\rangle \langle j|h_2|j'\rangle}{(\hbar\omega + \Delta_{jj''})(\hbar\omega + \Delta_{jj'})} \times (-1)^{j'+I-3} (2I+1) W(j'' I j' I; 23) \frac{\langle j''|\hat{\Omega}_p|j'\rangle}{\langle j|\hat{\Omega}_p|j\rangle} \right], \quad (12)$$

and

$$\Omega_c = -\frac{1}{28} R_0^2 g_R \frac{k^2 \hbar \omega}{C} \sum_{j'} \frac{\langle j | h_2 | j' \rangle^2}{(\hbar \omega + \Delta_{jj'})^2} \times \sum_{\mu=-2}^{\mu=2} \mu (17 - 5\mu^2) \langle j' 2I - \mu \mu | j' 2II \rangle^2. \quad (13)$$

Using the Bohr–Mottelson’s notation,  $\Delta_{jj'}$  is the energy difference of the particle levels with  $j$  and  $j'$ ,  $k$  is the coupling constant as defined in Eq. 5,  $W$  are the Racah coefficients,  $\langle j | h_2 | j' \rangle = \langle j || Y_2 || j' \rangle / \sqrt{2j+1}$ ,  $\Omega_{sp}$  is given by Eq. 3 and  $C$  is the nuclear deformability [44]

$$C_\lambda = (\lambda - 1)(\lambda + 2) R_0^2 S - \frac{3}{2\pi} \frac{\lambda - 1}{2\lambda + 1} \frac{Z^2 e^2}{R_0}, \quad (14)$$

where  $R_0$  is the radius of the nucleus and  $S$  is the surface tension. The analysis of nuclear binding energies leads to the estimate  $4\pi R_0^2 S = 15.4 A^{2/3}$  MeV [45] and  $\omega$  is the oscillation frequency of the surface

$$\omega = \sqrt{\frac{C_\lambda}{B_\lambda}}, \quad (15)$$

where using the classical hydrodynamical expression  $B_\lambda = \frac{1}{\lambda} \frac{3}{4\pi} AM R_0^2$  [44]. When  $\Delta_{jj'} (j' \neq j)$  is large and  $j$  may be considered a good quantum number,  $\Omega_c$  and  $\Omega_p$  are simplified as

$$\Omega_c = -\frac{45}{224\pi} g_R R_0^2 \frac{k^2}{\hbar \omega C} \cdot \frac{(2I - 1)(I - 1)}{I(I + 1)^2}, \quad (16)$$

and

$$\Omega_p = \Omega_{sp} \left[ 1 + \frac{5}{32\pi} \frac{k^2}{\hbar \omega C} (\mathcal{F}_1 - \mathcal{F}_2) \right], \quad (17)$$

where

$$\mathcal{F}_1 = \frac{4I^2(I + 1)^2 - 75I(I + 1) + 234}{4I^2(I + 1)^2}, \quad (18)$$

$$\mathcal{F}_2 = \frac{(2I - 1)(2I + 3)}{4I(I + 1)}. \quad (19)$$

### 3. Comparison with experimental results and predicted values for unmeasured cases

After this brief presentation of the models used for the deduction of  $\Omega$  a comparison is displayed between the predictions of each model and the very limited experimental results that are currently available. Experimental data have been retrieved from Fuller’s 1976 compilation [46] and cross-checked with the values published in the original works. Those data, as well as additional recent measurements that were collected from literature are about to be publicly available soon in the nuclear moments database, NUMOR [47, 48]. This assemble, to our knowledge, is the most complete collection of  $\Omega$  measurements. The predictions of each model along with the experimental values for the isotopes that their octupole moment has already been measured are presented in Tables 1 and 2 and in Figs. 1 and 2, as well. Some of the published data do not quote an experimental uncertainty and are marked with a  $b$  in Table 2.

We have used  $\langle r^2 \rangle = 3/5 R_0^2$ ,  $R_0 = 1.35 A^{1/3}$  fm [49], and  $k = 40$  MeV, while  $C$ ,  $\hbar \omega$  have been calculated from Eqs. 14 and 15.

As seen in Tables 1 and 2 the strong coupling case predicts the correct sign for most of the isotopes (except  $^{133}\text{Cs}$  and  $^{197}\text{Au}$ ). The same is true for the effective strong coupling case with the only exception being  $^{37}\text{Cl}$ . The case of  $^{87}\text{Rb}$  is special because many-body perturbation theory that is used for the extraction of  $\Omega$  from the hyperfine interaction constant  $c$  results in the different sign between the experimental value and the predictions of each model [10].

In a similar way, the weak coupling case predicts the correct sign for most of the isotopes (except  $^{133}\text{Cs}$ ,  $^{197}\text{Au}$ ,  $^{207}\text{Po}$  and  $^{209}\text{Bi}$ ). The same is true for the effective weak coupling case with the only exceptions being  $^{197}\text{Au}$  and  $^{207}\text{Po}$ . Moreover the strong coupling and the effective weak coupling case predicted exceptionally well the order of magnitude of  $\Omega$  for isotopes whose unpaired nucleon has spin  $I = l + 1/2$ , except  $^{45}\text{Sc}$  and  $^{155}\text{Gd}$ . However, in the case of  $^{155}\text{Gd}$ , the experimental value is only considered tentative [20]. The failure in describing isotopes whose unpaired nucleon has spin  $I = l - 1/2$  could be due to a cancellation between the orbital and spin contributions of the valence nucleon to the magnetic octupole moment in the basis of single particle model [4]. This observation, combined with the comment by Schwartz [6] that until more is known about polarization effects, the experimental values cannot be trusted for more than a qualitative comparison with the nuclear models, makes the strong coupling and the effective weak coupling cases very promising models for the description of  $\Omega$  for nuclei with spin  $I = l + 1/2$ .

It might be useful to examine a different approach in the grouping of the isotopes, based on which model or models should be applicable. One way to classify the nuclei is based on the  $R_{4/2}$  ratio in the even-even neighbor of the nuclide of interest. If  $R_{4/2} < 1$ , then a single-particle model should be most applicable; for  $R_{4/2} \sim 2$ , weak coupling is likely to be most appropriate. The strong coupling case should become applicable when  $R_{4/2} \sim 10/3$  [50]. Despite the fact that the distinction is not always clear cut the isotopes were divided into these three groups.

The first group is consisted by the isotopes  $^{87}\text{Rb}$  and  $^{209}\text{Bi}$  for which a single-particle model is expected to be most applicable. Based on the experimental values this is true, as either the extreme or the effective case of the single-particle model is the most accurate in their prediction.

The second group is consisted by isotopes  $^{155}\text{Gd}$  and  $^{173}\text{Yb}$  with  $R_{4/2} > 3$ . This value indicates well-deformed nucleus, consequently the strong coupling case is expected to be the most appropriate. While for  $^{155}\text{Gd}$  there is no success by any model, the case of  $^{173}\text{Yb}$  is different. In a recent paper published by de Groot *et al.* [22] there is no significant evidence for a non-zero octupole moment in  $^{173}\text{Yb}$ . As a result, the effective strong coupling case seems accurate in its prediction.

The third group is consisted by the remaining isotopes mentioned in Tables 1 and 2. For these isotopes the weak coupling case is expected to be the most applicable. While this is true for the majority of odd-proton nuclei, for odd-neutron nuclei the expected model based on  $R_{4/2}$  ratio has only occasionally predicted the correct order of magnitude for  $\Omega$ . More specifically, for nuclei  $^{131}\text{Xe}$ ,  $^{137}\text{Ba}^+$  and  $^{207}\text{Po}$  extreme or effective single-particle model predicted accurately their  $\Omega$  value in contrast with the weak coupling case. The same situation is observed for  $^{197}\text{Au}$ , while for nuclei  $^{45}\text{Sc}$  and  $^{133}\text{Cs}$  neither the weak coupling case nor any other model had any success in their prediction.

It is worth noting that both strong and weak coupling cases are successful in predicting the order of magnitude in several isotopes, with the weak coupling case having greater deviation from the experimental values. Interestingly, the opposite is true when the effective  $g$  factors have been incorporated in the calculations. The effective weak coupling case is clearly more successful in describing experimental data with respect to the effective strong coupling case (7 vs 2 isotopes). The prediction of the order of magnitude for the effective strong and weak coupling cases for isotopes with unpaired proton in subshell  $2p_{3/2}$ ,  $^{69,71}\text{Ga}$  and  $^{79,81}\text{Br}$  –except  $^{87}\text{Rb}$ , was also very good. In addition, the effective weak and strong coupling cases correctly predicted the order of magnitude for  $^{83}\text{Kr}$ ,  $^{127}\text{I}$  and  $^{201}\text{Hg}$ . These isotopes have more than 3 valence nucleons so the success could be possibly attributed to the increased impact of collective phenomena when moving away from magic numbers. However, there are other isotopes with 3 or more valence nucleons, such as

$^{35,37}\text{Cl}$  and  $^{197}\text{Au}$  that are not described correctly by the collective model.

Finally, there is a discrepancy of an order of magnitude between our theoretical predictions for  $\Omega_c$  (Eq. 16) and those originally reported by Suekane and Yamaguchi [30], for isotopes  $^{115}\text{In}$  and  $^{127}\text{I}$ .

The effective single particle model predictions for the majority of isotopes are more accurate than those for the extreme model. Moreover, the effective model predicted the correct order of magnitude of  $\Omega$  for most of the isotopes. Another interesting observation is that the effective single particle model predicted successfully the order of magnitude of  $\Omega$  for all the isotopes with  $A > 196$ . All of them have 3 or less valence nucleons, so the success of the effective single particle model could be due to their proximity to a closed-shell configuration. Most of these isotopes have spin  $I = l - 1/2$  and the effective single particle is the only model that has some accuracy in their prediction.

There is a general trend of the values of  $\Omega$  to fall inside the Schmidt lines of extreme single-particle model. However, there are isotopes such as  $^{45}\text{Sc}$ ,  $^{155}\text{Gd}$  and  $^{173}\text{Yb}$  that do not follow this trend and stress the need for further study, at both theoretical and experimental level.

It should be noted that both  $^{155}\text{Gd}$  and  $^{173}\text{Yb}$  are well-deformed nuclei in regions where their even-even cores are strongly collective with  $R_{4/2} > 3$ . In contrast,  $^{45}\text{Sc}$  nucleus with a single proton outside of the magic shell of  $Z = 20$  should be near spherical and calculable with the shell model. In [28] it is clear that despite the structure of  $^{45}\text{Sc}$  shell model calculations, including different interactions in a  $(sd)pf$ -shell model space, cannot reproduce its experimental value of  $\Omega$ .

In general, the usually smaller absolute value of experimental results compared to the extreme single-particle model predictions may be explained either by the configuration mixing method or the collective model.

If one takes the former, one has to introduce new configurations into the ground state which contribute to  $\Omega$ , but not to  $\mu$  and  $Q$  [30]. In a paper by Brown *et al.* [51],  $\Omega$  of isotopes  $^{35}\text{Cl}$  and  $^{37}\text{Cl}$  have been calculated from a complete  $sd$ -shell space wave functions using three sets of  $g$  factors. Their predictions using the free-nucleon  $g$  factors are in better agreement with the experimental values.

From the comparison of extreme single particle model and single particle model using effective  $g$  factors with the available experimental data it seems that the latter case describes the experimental values more accurately. Again, configuration mixing effects [52–57] can be possibly the reason. At this point it should be mentioned that we used effective  $g$  factors that are typically used in the  $M_1$  operator. The effective  $g$  factors in the  $M_3$  operator need not be identical to those in the  $M_1$  operator, but they will be related to the extent that they describe the same configuration mixing effects. It is reasonable to start by assuming that they are the same.

For the strong coupling case the reduction of  $\Omega$  is achieved via the projection factor  $P_3$  as seen in Eq. 7, which represents the transformation to the space fixed frame from the body fixed frame. The extremely limited experimental information available for  $\Omega$  available in 1957 were fitted by the collective model, using the strong coupling case. The additional experimental results that are available today seem to give the edge to the effective weak coupling case.

Concluding the application of the formalism discussed above, a complete set of values of the magnetic octupole moment for valence protons in subshells  $2p_{3/2}$  and  $1g_{9/2}$ , as well as valence neutrons in  $1g_{9/2}$  has been produced. The values are shown in detail in Tables 3, 4 and 5 where we have used the bare nucleon  $g$  factors, exclusively.



#### 4. Octupole moments and mirror nuclei

It is known that the sum of the ground-state magnetic moments of mirror nuclei can give valuable information about gross-spin properties of nuclei. More specifically, systematic trends in the spin expectation value as a function of the mass number for all  $T = 1/2, 3/2$  and  $5/2$  nuclei [43, 58–64] provide us with a valuable tool in predicting ground-state dipole magnetic moments of mirror partners. In a similar framework, a systematic study of magnetic octupole moments of mirror nuclei could reveal similar trends that have the potential to serve as a quick way in predicting  $\Omega$  of a nucleus if its mirror partner value is known experimentally.

The magnetic moment of a nucleus can be expressed in a formal way in the framework of the one-body magnetic moment operator with the help of the isospin formalism. By extending the work of Sugimoto [43, 65] we will express  $\Omega$  as an isoscalar and an isovector term.

Using the standard notation about expectation values,  $\Omega$  can be expressed as

$$\Omega = \left\langle \sum_i \left[ \frac{1}{2} (1 + \tau_3^i) \left( \nabla r^3 C_3^{(3)}(\theta, \phi) \right)_z \left( \frac{l_z^i}{2} + \sigma_z^i \mu_p \right) + \frac{1}{2} (1 - \tau_3^i) \left( \nabla r^3 C_3^{(3)}(\theta, \phi) \right)_z \sigma_z^i \mu_n \right] \right\rangle_{M=I}. \quad (20)$$

where  $\sigma$  stands for Pauli matrices,  $\tau$  for isospin (and its projection  $\tau_3$ ) and  $\mu_p$  and  $\mu_n$  denote the dipole magnetic moment of a free proton and neutron, respectively. The summation in  $i$  should be taken over all nucleons. This formula can be rewritten with an isoscalar and an isovector term

$$\Omega = \left\langle \sum_i \Omega_0^{(i)} \right\rangle_{M=I} + \left\langle \sum_i \Omega_3^{(i)} \right\rangle_{M=I}, \quad (21)$$

where

$$\Omega_0^{(i)} := \frac{1}{2} \left( \nabla r^3 C_3^{(3)}(\theta, \phi) \right)_z \left[ \frac{l_z^i}{2} + (\mu_p + \mu_n) \sigma_z^i \right], \quad (22)$$

$$\Omega_3^{(i)} := \frac{1}{2} \left( \nabla r^3 C_3^{(3)}(\theta, \phi) \right)_z \left[ \tau_3^i \frac{l_z^i}{2} + (\mu_p - \mu_n) \tau_3^i \sigma_z^i \right]. \quad (23)$$

Under the assumptions that the isospin is a good quantum number, there is charge symmetry in nuclear forces, and the Coulomb interaction can be neglected, for a pair of mirror states the expectation values  $\left\langle \sum_i \Omega_0^{(i)} \right\rangle_{M=I}$  are independent of  $T_3$ , while the expectation values  $\left\langle \sum_i \Omega_3^{(i)} \right\rangle_{M=I}$  differ only in sign for  $T_3 = \pm T$ . Therefore, the sum of octupole moments of mirror states

$$\begin{aligned} \Omega(T_3 = +T) + \Omega(T_3 = -T) &= 2 \left\langle T, T_3 = +T \left| \sum_i \Omega_0^{(i)} \right| T, T_3 = +T \right\rangle, \\ &= \frac{1}{2} \left\langle \sum_i \left( \nabla r^3 C_3^{(3)}(\theta, \phi) \right)_z l_z^{(i)} \right\rangle_{M=I} + (\mu_p + \mu_n) \left\langle \sum_i \left( \nabla r^3 C_3^{(3)}(\theta, \phi) \right)_z \sigma_z^{(i)} \right\rangle_{M=I}. \end{aligned} \quad (24)$$

The operators  $\left( \nabla r^3 C_3^{(3)}(\theta, \phi) \right)_z$  and  $\sigma_z^{(i)}$  are acting in different Hilbert spaces, therefore their expectation values can be separated. The goal is to express the sum of  $\Omega$  of mirror states as a function of spin expectation value  $\langle \sum_i \sigma_z^{(i)} \rangle_{M=I}$  or differently written  $\langle \sigma \rangle$ . In order to achieve that, it is essential to express the expectation value of the operator  $\sum_i \left( \nabla r^3 C_3^{(3)}(\theta, \phi) \right)_z l_z^{(i)}$  as a function of  $\langle \sigma \rangle$  and  $\left\langle \left( \nabla r^3 C_3^{(3)}(\theta, \phi) \right)_z \right\rangle$ .

This may be solved by using the Racah technique with the use of which the Eq. 54 in Ref. [31] is derived for the matrix elements

$$\left\langle l \frac{1}{2} I \left| \nabla (g C_k) \cdot (g_l \mathbf{L} + g_s \mathbf{S}) \right| l' \frac{1}{2} I' \right\rangle,$$

where  $g$  is any function of  $r$ .

By defining  $\Xi$  as the expectation value of the matrix that is composed of these matrix elements, we can derive the following relations

$$\left\langle \left| \left( \nabla r^3 C_3^{(3)}(\theta, \phi) \right)_z g l_z^{(i)} \right| \right\rangle = \Xi - \left\langle \left| \left( \nabla r^3 C_3^{(3)}(\theta, \phi) \right)_z \right| \right\rangle \frac{g_s}{2} \langle \sigma \rangle. \quad (25)$$

It is easy to understand that there will be a linear relation between  $\langle \sigma \rangle$  and the sum of  $\Omega$  expressed in Eq. 24. Consequently, knowing the exact values of magnetic octupole moment for pairs of mirror nuclei could reveal systematic trends in the spin expectation value as a function of the mass number for nuclei with the same isospin. As a result, the cases of  $^{35}\text{Ar}$  and  $^{37}\text{Ca}$  are particularly interesting for measuring, as they are the mirror nuclei of the already measured  $^{35,37}\text{Cl}$ . As of now, there is no experimental information about  $\Omega$  of any pair of mirror nuclei that could ascertain this conversation. Still, the discussion is considered useful for future experimental and theoretical research along these lines.

## 5. Conclusions

The octupole moment is revisited as a nuclear observable which can draw more attention in the near future at both experimental and theoretical level. Old and recent experimental data of magnetic octupole moments have been searched and collected in an updated compilation.

Theoretical modeling seems to suggest that the collective model is more favorable to describe the presently available experimental  $\Omega$  data compared to the extreme single-particle model. Both strong and weak coupling cases predict the correct sign of  $\Omega$  for the vast majority of nuclei. More importantly, both of these cases predict correctly the order of magnitude of  $\Omega$  for the majority of nuclei with spin  $I = l + 1/2$ . In particular, nuclei with valence proton in the  $2p_{3/2}$  or in the  $1g_{9/2}$  subshell seem to be described slightly better by considering the effective weak coupling case. The same is true for  $^{127}\text{I}$  with valence protons in subshell  $2d_{5/2}$ . More data in this subshell are required to attempt a more general conclusion.

Furthermore, the case of  $^{45}\text{Sc}$ , a nucleus with valence proton in subshell  $1f_{7/2}$  is not described correctly by either the strong or the weak coupling cases. This is in agreement with recent investigations by de Groote *et al.* [28]. Finally, the strong coupling scheme seems to deviate more than the effective weak coupling one for about 60% of the nuclei with spin  $I = l + 1/2$ . As a result, despite it is quite difficult to give the edge to either of them, using the most recent and updated measurements, the effective weak coupling case seems to gain ground in the theoretical description over the strong coupling case, challenging the conclusion drawn by Suekane and Yamaguchi [30].

At this point it is important to highlight that the majority of the isotopes, whose  $\Omega$  has been measured, are in regions where their even-even cores are weakly collective with  $R_{4/2} \sim 2$ . One should expect that effective weak coupling case would be the most successful model in describing these isotopes. While, this is true for odd-proton nuclei, for odd-neutron nuclei the expected model based on  $R_{4/2}$  ratio has only occasionally predicted the correct order of magnitude for  $\Omega$ .

This work has additionally produced a set of predictions for more than 100 nuclei, which are proposed as starting values for future experimental studies. As the relevant experimental methods in radioactive beam facilities gain more power and efficiency in accessing such nuclear observables, this list may be useful for researchers in nuclear structure, both experimentally and theoretically.

## Acknowledgements

We thank Dr. D. Bonatsos for providing feedback on the manuscript and V. Bofos for useful discussions.

## References

- [1] N. J. Stone, Table of Recommended Nuclear Magnetic Dipole Moments: Part I - Long-lived States, Technical Report, IAEA, 2019. doi:[0.61092/iaea.yjpc-cns6](https://doi.org/0.61092/iaea.yjpc-cns6).
- [2] N. J. Stone, Table of Recommended Nuclear Magnetic Dipole Moments - Part II, Short-lived States, Technical Report, IAEA, 2020. doi:[10.61092/iaea.1p48-p6c6](https://doi.org/10.61092/iaea.1p48-p6c6).
- [3] N. J. Stone, Table of Nuclear Electric Quadrupole Moments, Technical Report, IAEA, 2021. doi:[10.61092/iaea.a6te-dg7q](https://doi.org/10.61092/iaea.a6te-dg7q).
- [4] K. Beloy, A. Derevianko, V. A. Dzuba, G. T. Howell, B. B. Blinov, E. N. Fortson, Nuclear magnetic octupole moment and the hyperfine structure of the  $5D_{3/2,5/2}$  states of the  $Ba^+$  ion, Phys. Rev. A 77 (2008) 052503. doi:[10.1103/PhysRevA.77.052503](https://doi.org/10.1103/PhysRevA.77.052503).
- [5] J. Dobaczewski, J. Engel, M. Kortelainen, P. Becker, Correlating Schiff moments in the light actinides with octupole moments, Phys. Rev. Lett. 121 (2018) 232501. doi:[10.1103/PhysRevLett.121.232501](https://doi.org/10.1103/PhysRevLett.121.232501).
- [6] C. Schwartz, Theory of hyperfine structure, Phys. Rev. 105 (1957) 173–183. doi:[10.1103/PhysRev.105.173](https://doi.org/10.1103/PhysRev.105.173).
- [7] M. J. Amoruso, W. R. Johnson, Relativistic one-electron calculations of shielded atomic hyperfine constants, Phys. Rev. A 3 (1971) 6–12. doi:[10.1103/PhysRevA.3.6](https://doi.org/10.1103/PhysRevA.3.6).
- [8] J. R. Zacharias, J. G. King, C. L. Searle, S. Ketudat, R. F. C. Vessot, D. D. Babb, V. J. Bates, H. H. Brown Jr, B. DiBartolo, D. S. Edmonds Jr, et al., Vii. atomic beams, Quarterly Progress Report (1955).
- [9] H. H. Brown, J. G. King, Hyperfine structure and octopole interaction in stable bromine isotopes, Phys. Rev. 142 (1966) 53–59. doi:[10.1103/PhysRev.142.53](https://doi.org/10.1103/PhysRev.142.53).
- [10] V. Gerginov, C. E. Tanner, W. R. Johnson, Observation of the nuclear magnetic octupole moment of  $^{87}\text{Rb}$  from spectroscopic measurements of hyperfine intervals, Can. J. Phys. 87 (2009) 101–104. doi:[10.1139/p08-145](https://doi.org/10.1139/p08-145).
- [11] T. G. Eck, P. Kusch, Hfs of the  $5^2p_{3/2}$  state of  $\text{In}^{115}$  and  $\text{In}^{113}$ : Octupole interactions in the stable isotopes of indium, Phys. Rev. 106 (1957) 958–964. doi:[10.1103/PhysRev.106.958](https://doi.org/10.1103/PhysRev.106.958).
- [12] V. Gerginov, A. Derevianko, C. Tanner, Observation of the nuclear magnetic octupole moment of Cs-133, Phys. Rev. Lett. 91 (2003) 072501. doi:[10.1103/PhysRevLett.91.072501](https://doi.org/10.1103/PhysRevLett.91.072501).
- [13] A. G. Blachman, D. A. Landman, A. Lurio, Hyperfine structure and  $g_J$  value of the  $^2D_{3/2}$  and of the  $^4F_{7/2}$  states of  $\text{Au}^{197}$ , Phys. Rev. 161 (1967) 60–67. doi:[10.1103/PhysRev.161.60](https://doi.org/10.1103/PhysRev.161.60).
- [14] D. A. Landman, A. Lurio, Hyperfine structure of the  $(6p)^3$  configuration of  $\text{Bi}^{209}$ , Phys. Rev. A 1 (1970) 1330–1338. doi:[10.1103/PhysRevA.1.1330](https://doi.org/10.1103/PhysRevA.1.1330).
- [15] W. L. Faust, L. Y. Chow Chiu, Hyperfine structure of the metastable  $(4p)^5(5s)^3P_2$  state of  $^{83}\text{Kr}$ , Phys. Rev. 129 (1963) 1214–1220. doi:[10.1103/PhysRev.129.1214](https://doi.org/10.1103/PhysRev.129.1214).

- [16] W. L. Faust, M. N. McDermott, Hyperfine structure of the  $(5p)^5(6s)^3P_2$  state of  ${}_{54}\text{Xe}^{129}$  and  ${}_{54}\text{Xe}^{131}$ , Phys. Rev. 123 (1961) 198–204. doi:[10.1103/PhysRev.123.198](https://doi.org/10.1103/PhysRev.123.198).
- [17] N. C. Lewty, B. L. Chuah, R. Cazan, M. D. Barrett, B. K. Sahoo, Experimental determination of the nuclear magnetic octupole moment of  ${}^{137}\text{Ba}^+$  ion, Phys. Rev. A 88 (2013) 012518. doi:[10.1103/PhysRevA.88.012518](https://doi.org/10.1103/PhysRevA.88.012518).
- [18] N. C. Lewty, B. L. Chuah, R. Cazan, B. K. Sahoo, M. D. Barrett, Spectroscopy on a single trapped  ${}^{137}\text{Ba}^+$  ion for nuclear magnetic octupole moment determination: erratum, Opt. Express 21 (2013) 7131–7132. doi:[10.1364/OE.21.007131](https://doi.org/10.1364/OE.21.007131).
- [19] M. R. Hoffman, Observation of the Nuclear Magnetic Octupole Moment of  ${}^{137}\text{Ba}^+$ , Ph.D. thesis, Washington University, 2014. URL: <http://hdl.handle.net/1773/27558>.
- [20] P. J. Unsworth, Nuclear dipole, quadrupole and octupole moments of  ${}^{155}\text{Gd}$  by atomic beam magnetic resonance, J. Phys. B 2 (1969) 122–133. doi:[10.1088/0022-3700/2/1/318](https://doi.org/10.1088/0022-3700/2/1/318).
- [21] A. K. Singh, D. Angom, V. Natarajan, Observation of the nuclear magnetic octupole moment of  ${}^{173}\text{Yb}$  from precise measurements of the hyperfine structure in the  ${}^3P_2$  state, Phys. Rev. A 87 (2013) 012512. doi:[10.1103/PhysRevA.87.012512](https://doi.org/10.1103/PhysRevA.87.012512).
- [22] R. P. de Groote, S. Kujanpää, A. Koszorús, J. G. Li, I. D. Moore, Magnetic octupole moment of  ${}^{173}\text{Yb}$  using collinear laser spectroscopy, Phys. Rev. A 103 (2021) 032826. doi:[10.1103/PhysRevA.103.032826](https://doi.org/10.1103/PhysRevA.103.032826).
- [23] M. N. McDermott, W. L. Lichten, Hyperfine structure of the  $6^3P_2$  state of  ${}_{80}\text{Hg}^{199}$  and  ${}_{80}\text{Hg}^{201}$ . Properties of metastable states of mercury, Phys. Rev. 119 (1960) 134–143. doi:[10.1103/PhysRev.119.134](https://doi.org/10.1103/PhysRev.119.134).
- [24] C. M. Olsmats, S. Axensten, G. Liljegren, Hyperfine structure investigation of Po-205 and Po-207, Arkiv for Fysik 19 (1961) 469–481.
- [25] R. T. Daly, J. H. Holloway, Nuclear magnetic octupole moments of the stable Gallium isotopes, Phys. Rev. 96 (1954) 539–540. doi:[10.1103/PhysRev.96.539](https://doi.org/10.1103/PhysRev.96.539).
- [26] V. Jaccarino, J. G. King, R. A. Satten, H. H. Stroke, Hyperfine structure of  $\text{I}^{127}$ . nuclear magnetic octupole moment, Phys. Rev. 94 (1954) 1798–1799. doi:[10.1103/PhysRev.94.1798](https://doi.org/10.1103/PhysRev.94.1798).
- [27] R. J. Hull, G. O. Brink, Hyperfine structure of  $\text{Bi}^{209}$ , Phys. Rev. A 1 (1970) 685–693. doi:[10.1103/PhysRevA.1.685](https://doi.org/10.1103/PhysRevA.1.685).
- [28] R. P. de Groote, J. Moreno, J. Dobaczewski, Á. Koszorús, I. Moore, M. Reponen, B. Sahoo, C. Yuan, Precision measurement of the magnetic octupole moment in  ${}^{45}\text{Sc}$  as a test for state-of-the-art atomic-and nuclear-structure theory, Physics Letters B 827 (2022) 136930.
- [29] A. Rosén, Hyperfine structure analysis for the ground configuration of bismuth, Phys. Scr. 6 (1972) 37–46. doi:[10.1088/0031-8949/6/1/004](https://doi.org/10.1088/0031-8949/6/1/004).
- [30] S. Suekane, Y. Yamaguchi, The Magnetic Octupole Moments of Nuclei, Prog. Theor. Phys. 17 (1957) 443–448. doi:[10.1143/PTP.17.443](https://doi.org/10.1143/PTP.17.443).
- [31] C. Schwartz, Theory of hyperfine structure, Phys. Rev. 97 (1955) 380–395. doi:[10.1103/PhysRev.97.380](https://doi.org/10.1103/PhysRev.97.380).
- [32] S. J. Zhu, Q. H. Lu, J. H. Hamilton, A. V. Ramayya, L. K. Peker, M. G. Wang, W. C. Ma, B. R. S. Babu, T. N.

- Ginter, J. Kormicki, D. Shi, J. K. Deng, W. Nazarewicz, J. O. Rasmussen, M. A. Stoyer, S. Y. Chu, K. E. Gregorich, M. F. Mohar, S. Asztalos, S. G. Prussin, J. D. Cole, R. Aryaeinejad, Y. K. Dardenne, M. Drigert, K. J. Moody, R. W. Loughed, J. F. Wild, N. R. Johnson, I. Y. Lee, F. K. McGowan, G. M. Ter-Akopian, Y. T. Oganessian, Octupole deformation in  $^{142,143}\text{Ba}$  and  $^{144}\text{Ce}$ : new band structures in neutron-rich Ba-isotopes, *Phys. Lett. B* 357 (1995) 273 – 280. doi:[10.1016/0370-2693\(95\)00900-6](https://doi.org/10.1016/0370-2693(95)00900-6).
- [33] N. Auerbach, V. V. Flambaum, V. Spevak, Collective t- and p-odd electromagnetic moments in nuclei with octupole deformations, *Phys. Rev. Lett.* 76 (1996) 4316–4319. doi:[10.1103/PhysRevLett.76.4316](https://doi.org/10.1103/PhysRevLett.76.4316).
- [34] D. Bonatsos, D. Lenis, N. Minkov, D. Petrellis, P. Yotov, Analytic description of critical-point actinides in a transition from octupole deformation to octupole vibrations, *Phys. Rev. C* 71 (2005) 064309. doi:[10.1103/PhysRevC.71.064309](https://doi.org/10.1103/PhysRevC.71.064309).
- [35] N. Minkov, P. Yotov, S. Drenska, W. Scheid, D. Bonatsos, D. Lenis, D. Petrellis, Nuclear collective motion with a coherent coupling interaction between quadrupole and octupole modes, *Phys. Rev. C* 73 (2006) 044315. doi:[10.1103/PhysRevC.73.044315](https://doi.org/10.1103/PhysRevC.73.044315).
- [36] L. M. Robledo, G. F. Bertsch, Global systematics of octupole excitations in even-even nuclei, *Physical Review C* 84 (2011) 054302.
- [37] L. P. Gaffney, P. A. Butler, M. Scheck, A. B. Hayes, F. Wenander, M. Albers, B. Bastin, C. Bauer, A. Blazhev, S. Bönig, N. Bree, J. Cederkäll, T. Chupp, D. Cline, T. E. Cocolios, T. Davinson, H. De Witte, J. Diriken, T. Grahn, A. Herzan, M. Huysse, D. G. Jenkins, D. T. Joss, N. Kesteloot, J. Konki, M. Kowalczyk, T. Kröll, E. Kwan, R. Lutter, K. Moschner, P. Napiorkowski, J. Pakarinen, M. Pfeiffer, D. Radeck, P. Reiter, K. Reynders, S. V. Rigby, L. M. Robledo, M. Rudigier, S. Sambhi, M. Seidlitz, B. Siebeck, T. Stora, P. Thoele, P. Van Duppen, M. J. Vermeulen, M. von Schmid, D. Voulot, N. Warr, K. Wimmer, K. Wrzosek-Lipska, C. Y. Wu, M. Zielinska, Studies of pear-shaped nuclei using accelerated radioactive beams, *Nature* 497 (2013) 199–204. doi:[10.1038/nature12073](https://doi.org/10.1038/nature12073).
- [38] D. Bonatsos, A. Martinou, N. Minkov, S. Karampagia, D. Petrellis, Octupole deformation in light actinides within an analytic quadrupole octupole axially symmetric model with a davidson potential, *Phys. Rev. C* 91 (2015) 054315. doi:[10.1103/PhysRevC.91.054315](https://doi.org/10.1103/PhysRevC.91.054315).
- [39] N. T. Brewer, E. H. Wang, W. A. Yzaguirre, J. H. Hamilton, A. V. Ramayya, S. H. Liu, J. K. Hwang, Y. X. Luo, C. J. Zachary, J. O. Rasmussen, S. J. Zhu, C. Goodin, G. M. Ter-Akopian, A. V. Daniel, Y. T. Oganessian, Octupole Deformation in  $^{144}\text{Ba}$  and  $^{148}\text{Ce}$ , 2018, pp. 197–202. doi:[10.1142/9789813229426\\_0038](https://doi.org/10.1142/9789813229426_0038).
- [40] P. A. Butler, L. P. Gaffney, P. Spagnoletti, K. Abrahams, M. Bowry, J. Cederkäll, G. de Angelis, H. De Witte, P. E. Garrett, A. Goldkuhle, C. Henrich, A. Illana, K. Johnston, D. T. Joss, J. M. Keatings, N. A. Kelly, M. Komorowska, J. Konki, T. Kröll, M. Lozano, B. S. Nara Singh, D. O'Donnell, J. Ojala, R. D. Page, L. G. Pedersen, C. Raison, P. Reiter, J. A. Rodriguez, D. Rosiak, S. Rothe, M. Scheck, M. Seidlitz, T. M. Shneidman, B. Siebeck, J. Sinclair, J. F. Smith, M. Stryjczyk, P. Van Duppen, S. Vinals, V. Virtanen, N. Warr, K. Wrzosek-Lipska, M. Zielińska, Evolution of octupole deformation in radium nuclei from coulomb excitation of radioactive  $^{222}\text{Ra}$  and  $^{228}\text{Ra}$  beams, *Phys. Rev. Lett.* 124 (2020) 042503. doi:[10.1103/PhysRevLett.124.042503](https://doi.org/10.1103/PhysRevLett.124.042503).
- [41] C. R. Chinn, A. S. Umar, M. Vallieres, M. R. Strayer, Mean field studies of exotic nuclei, *Physics reports* 264

- (1996) 107–121.
- [42] R. A. Sen'kov, V. F. Dmitriev, Nuclear magnetization distribution and hyperfine splitting in  $\text{Bi}^{82+}$  ion, *Nucl. Phys. A* 706 (2002) 351 – 364. doi:[10.1016/S0375-9474\(02\)00759-5](https://doi.org/10.1016/S0375-9474(02)00759-5).
- [43] T. J. Mertzimekis, Prediction and evaluation of magnetic moments in  $t = 1/2, 3/2,$  and  $5/2$  mirror nuclei, *Phys. Rev. C* 94 (2016) 064313. doi:[10.1103/PhysRevC.94.064313](https://doi.org/10.1103/PhysRevC.94.064313).
- [44] A. N. Bohr, B. R. Mottelson, Collective and individual-particle aspects of nuclear structure, *Dan. Mat. Fys. Medd.* 27 (1953) 1–174.
- [45] L. Rosenfeld, *Nuclear Forces*, North-Holland, 1948.
- [46] G. H. Fuller, Nuclear spins and moments, *J. Phys. Chem. Ref. Data* 5 (1976) 835–1092. doi:[10.1063/1.555544](https://doi.org/10.1063/1.555544).
- [47] T. J. Mertzimekis, K. Stamou, A. Psaltis, An online database of nuclear electromagnetic moments, *Nucl. Instrum. Meth. Phys. Res. A* 807 (2016) 56–60. doi:[10.1016/j.nima.2015.10.096](https://doi.org/10.1016/j.nima.2015.10.096).
- [48] T. J. Mertzimekis, S. Pelonis, K. Papanastasopoulos, An upgrade of the nuclear moments database NUMOR (2024). (in prep.).
- [49] K. K. Seth, D. J. Hughes, R. L. Zimmerman, R. C. Garth, Nuclear radii by scattering of low-energy neutrons, *Phys. Rev.* 110 (1958) 692–700. doi:[10.1103/PhysRev.110.692](https://doi.org/10.1103/PhysRev.110.692).
- [50] R. F. Casten, N. V. Zamfir, D. S. Brenner, A new simple global phenomenology of nuclear shape transitions, in: *Proceedings of the International Conference on radioactive nuclear beams, 24-27 May 1993*; URL: <https://www.osti.gov/biblio/10172873>.
- [51] B. A. Brown, W. Chung, B. H. Wildenthal, Electromagnetic multipole moments of ground states of stable odd-mass nuclei in the sd shell, *Physical Review C* 22 (1980) 774.
- [52] H. Noya, A. Arima, H. Horie, Nuclear moments and configuration mixing, *Progress of Theoretical Physics Supplement* 8 (1958) 33–112.
- [53] A. G. M. Van Hees, P. W. M. Glaudemans, Effects of configuration mixing on predominantly  $7/2^+$  states in  $a = 52$ – $55$  nuclei, *Zeitschrift für Physik A Atoms and Nuclei* 303 (1981) 267–276.
- [54] A. Wolf, R. F. Casten, Effective valence proton and neutron numbers in transitional  $a \cong 150$  nuclei from  $b(e2)$  and  $g$ -factor data, *Physical Review C* 36 (1987) 851.
- [55] J. D. Vergados, Configuration mixing effects on  $m1$  transitions and magnetic moments in pb region, *Physics Letters B* 36 (1971) 12–17.
- [56] T. J. Mertzimekis, A. E. Stuchbery, N. Benczer-Koller, M. J. Taylor, Systematics of first  $2^+$  state  $g$  factors around mass 80, *Physical Review C* 68 (2003) 054304.
- [57] A. E. Stuchbery, G. J. Lampard, H. H. Bolotin, Transient field measurements of  $g$ -factors in 194,196,198 pt;  $g(21^+)$  systematics in transitional w, os, pt nuclei, *Nuclear Physics A* 528 (1991) 447–464.
- [58] B. Buck, S. M. Perez, New look at magnetic moments and beta decays of mirror nuclei, *Phys. Rev. Lett.* 50 (1983) 1975–1978. doi:[10.1103/PhysRevLett.50.1975](https://doi.org/10.1103/PhysRevLett.50.1975).

- [59] B. Buck, A. C. Merchant, S. M. Perez, Magnetic moments of mirror nuclei, *Phys. Rev. C* 63 (2001) 037301. doi:[10.1103/PhysRevC.63.037301](https://doi.org/10.1103/PhysRevC.63.037301).
- [60] S. S. Hanna, J. W. Hugg, Analysis of the magnetic moments of mirror nuclei, *Hyperfine Interact.* 21 (1985) 59–77. doi:[10.1007/BF02061977](https://doi.org/10.1007/BF02061977).
- [61] T. J. Mertzimekis, P. F. Mantica, A. D. Davies, S. N. Liddick, B. E. Tomlin, Ground state magnetic dipole moment of  $^{35}\text{K}$ , *Phys. Rev. C* 73 (2006) 024318. doi:[10.1103/PhysRevC.73.024318](https://doi.org/10.1103/PhysRevC.73.024318).
- [62] J. S. Berryman, K. Minamisono, W. F. Rogers, B. A. Brown, H. L. Crawford, G. F. Grinyer, P. F. Mantica, J. B. Stoker, I. S. Towner, Doubly-magic nature of  $^{56}\text{Ni}$ : Measurement of the ground state nuclear magnetic dipole moment of  $^{55}\text{Ni}$ , *Phys. Rev. C* 79 (2009) 064305. doi:[10.1103/PhysRevC.79.064305](https://doi.org/10.1103/PhysRevC.79.064305).
- [63] S. M. Perez, W. A. Richter, B. A. Brown, M. Horoi, Correlations between magnetic moments and  $\beta$  decays of mirror nuclei, *Phys. Rev. C* 77 (2008) 064311. doi:[10.1103/PhysRevC.77.064311](https://doi.org/10.1103/PhysRevC.77.064311).
- [64] K. Minamisono, P. F. Mantica, T. J. Mertzimekis, A. D. Davies, M. Hass, J. Pereira, J. S. Pinter, W. F. Rogers, J. B. Stoker, B. E. Tomlin, R. R. Weerasiri, Nuclear magnetic moment of the  $^{57}\text{Cu}$  ground state, *Phys. Rev. Lett.* 96 (2006) 102501. doi:[10.1103/PhysRevLett.96.102501](https://doi.org/10.1103/PhysRevLett.96.102501).
- [65] K. Sugimoto, Magnetic moments and  $\beta$ -decay ft values of mirror nuclei, *Phys. Rev.* 182 (1969) 1051–1054. doi:[10.1103/PhysRev.182.1051](https://doi.org/10.1103/PhysRev.182.1051).
- [66] F. G. Kondev, M. Wang, W. J. Huang, S. Naimi, G. Audi, The *nubase2020* evaluation of nuclear physics properties, *Chinese Physics C* 45 (2021) 030001. doi:[10.1088/1674-1137/abddae](https://doi.org/10.1088/1674-1137/abddae).

## Figures

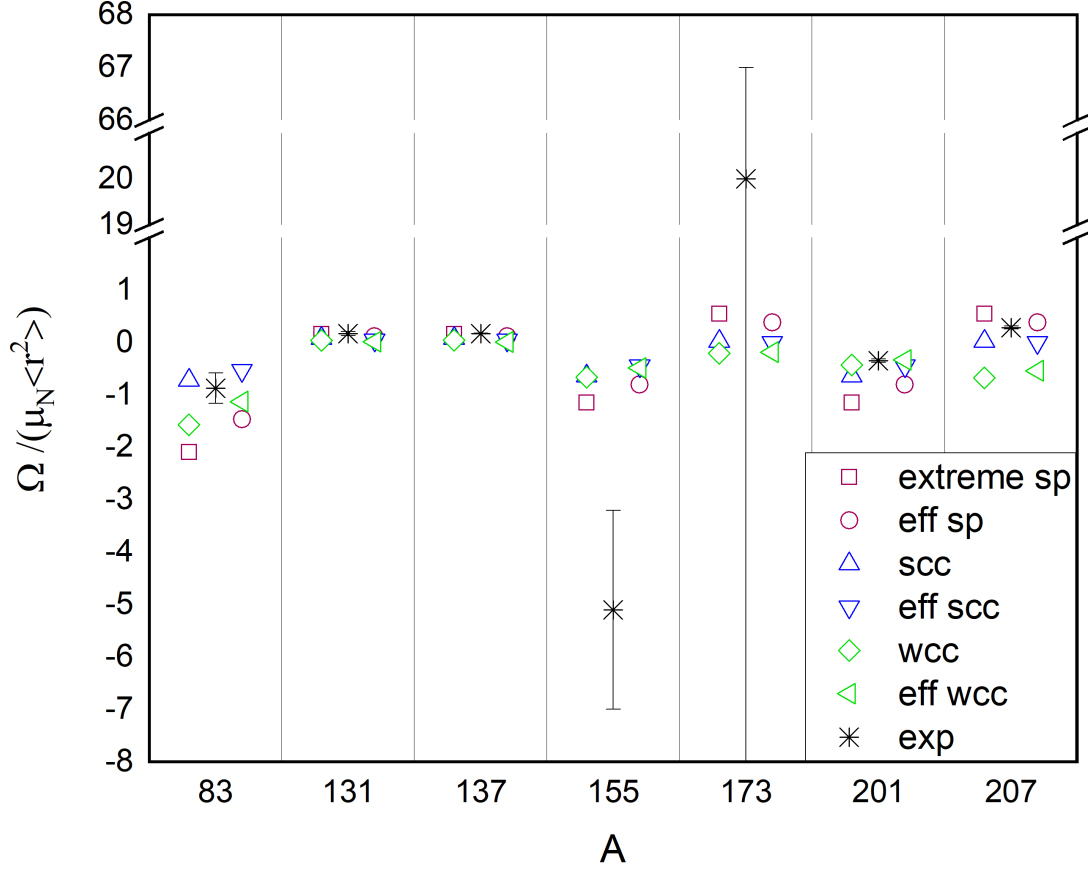


**Fig. 1:** Visual comparison of experimental results (*exp*) for  $\Omega$  and the predictions of extreme and effective (*eff*) single particle model (*sp*, magenta), strong (*scc*, blue) and weak (*wcc*, green) coupling case for nuclei with unpaired neutron, respectively. For better visualization, the points of *eff sp*, *eff scc* and *eff wcc* have been moved slightly to the right. The case of  $^{173}\text{Yb}$  is not presented in the diagram. For some isotopes the error bars are smaller than the size of the plotted points. Please note that the x-axis is not linear, while the y-axis includes breaks at two values to include the distinctively high value of  $^{173}\text{Yb}$  together with the rest of the plotted data.



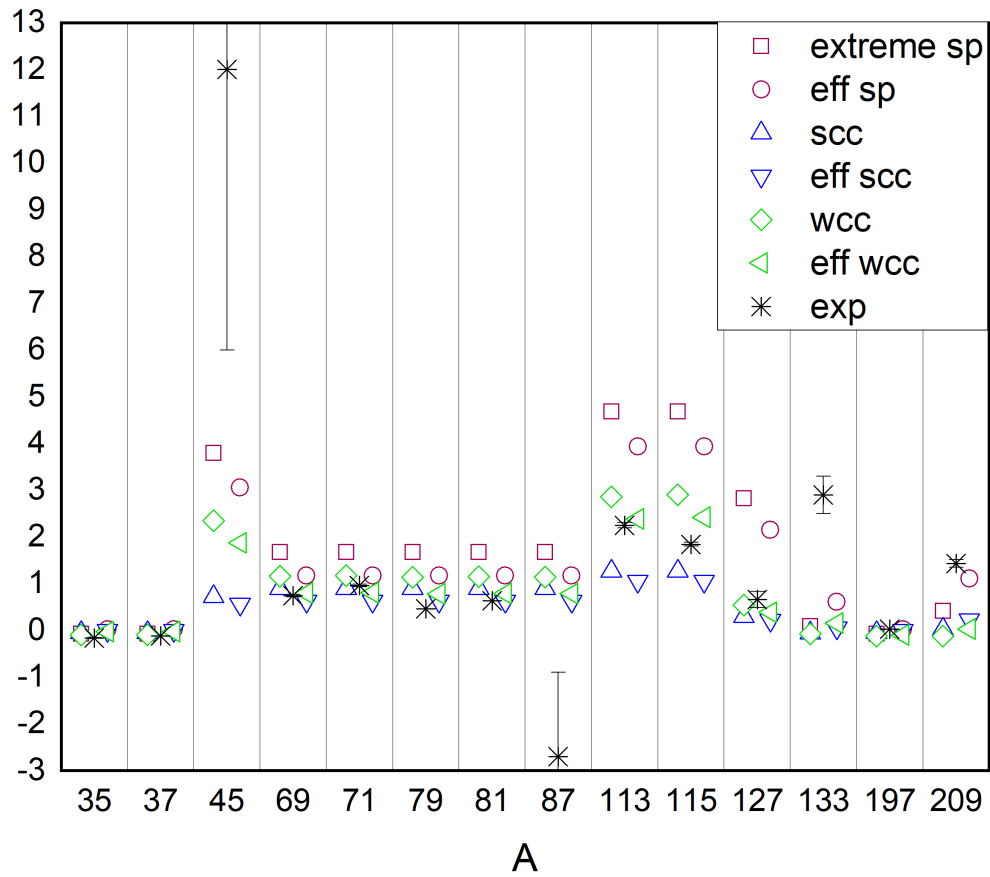


**Fig. 2:** Visual comparison of experimental results (*exp*) for  $\Omega$  and the predictions of extreme and effective (*eff*) single particle model (*sp*, magenta), strong (*scc*, blue) and weak (*wcc*, green) coupling case for nuclei with an unpaired proton, respectively. For better visualization, the points of *eff sp*, *eff scc* and *eff wcc* have been moved slightly to the right. For some isotopes the error bars are smaller than the size of the plotted points. The values for  $^{79}\text{Br}$  and  $^{81}\text{Br}$  have no cited uncertainty in literature. Please note that the x-axis is not linear.

## Explanation of Tables

**Table 1. Comparison between experimental and theoretical values of magnetic octupole moments for odd-neutron nuclei.**

Comparison between experimental (*exp*) and theoretical (single-particle (*s.p.*) and collective strong (*scc*) and weak (*wcc*) coupling) values of magnetic octupole moments for odd-neutron nuclei. The equations used to calculate the various  $\Omega$  values are listed in the first row.  $\Omega/\langle r^2 \rangle$  is expressed in unit of  $\mu_N$ . The second value quoted for each isotope has been calculated with effective values  $g_s^{eff} = 0.7g_s$  and  $g_l^{eff} = g_l + \delta g_l$ , where  $\delta g_l = +0.1$  for an unpaired proton and  $\delta g_l = 0.0$  for an unpaired neutron.

Isotope	Experimental and theoretical values of magnetic octupole moments of odd-neutron isotopes
$I^\pi$	Spin and parity of the state (from Ref. [66])
Shell assign.	Shows the shell assignment for each isotope
Experimental	Available experimental data in literature (see next column on the right for the corresponding published works). Notation is as follows: <ul style="list-style-type: none"> <li>(a) This value has been used in Fig. 1</li> <li>(b) The different sign is a result of a different convention of how the octupole moment is related to the hyperfine <math>C</math> constant</li> </ul>
Ref.	References to literature with experimental values of magnetic octupole moments
s.p. model	Single-particle model calculations, $\Omega_{sp}/\langle r^2 \rangle$ (via Eq. 3)
Collective model	Calculated octupole moments with the collective model. <ul style="list-style-type: none"> <li>Two calculations involved strong coupling: <ul style="list-style-type: none"> <li><math>\Omega_o/\langle r^2 \rangle</math> (via Eq. 9),</li> <li><math>\Omega_{scc}/\langle r^2 \rangle</math> (via Eqs. 7 and 10),</li> </ul> </li> <li>while three involved weak coupling: <ul style="list-style-type: none"> <li><math>\Omega_p/\langle r^2 \rangle</math> (via Eq. 17)</li> <li><math>\Omega_c/\langle r^2 \rangle</math> (via Eq. 16), and</li> <li><math>\Omega_{wcc}/\langle r^2 \rangle</math> (via Eq. 11), respectively.</li> </ul> </li> </ul>

**Table 2. Comparison between experimental and theoretical values of magnetic octupole moments for odd-proton nuclei.**

Comparison between experimental (*exp*) and theoretical (single-particle (*s.p.*) and collective strong (*scc*) and weak (*wcc*) coupling) values of magnetic octupole moments for odd-proton nuclei. The equations used to calculate the various  $\Omega$  values are listed in the first row.  $\Omega/\langle r^2 \rangle$  is expressed in unit of  $\mu_N$ . The second value quoted for each isotope has been calculated with effective values  $g_s^{eff} = 0.7g_s$  and  $g_l^{eff} = g_l + \delta g_l$ , where  $\delta g_l = +0.1$  for an unpaired proton and  $\delta g_l = 0.0$  for an unpaired neutron.

Isotope	Experimental and theoretical values of magnetic octupole moments of odd-proton isotopes
$I^\pi$	Spin and parity of the state (from Ref. [66])
Shell assign.	Shows the shell assignment for each isotope
Experimental	Available experimental data in literature (see next column on the right for the corresponding published works). Notation is as follows: (a) This value has been used in Fig. 2 (b) No cited experimental uncertainty in literature
Ref.	References to literature with experimental values of magnetic octupole moments
s.p. model	Single-particle model calculations, $\Omega_{sp}/\langle r^2 \rangle$ (via Eq. 3)
Collective model	Calculated octupole moments with the collective model. Two calculations involved strong coupling: $\Omega_o/\langle r^2 \rangle$ (via Eq. 9), $\Omega_{scc}/\langle r^2 \rangle$ (via Eqs. 7 and 10), while three involved weak coupling: $\Omega_p/\langle r^2 \rangle$ (via Eq. 17) $\Omega_c/\langle r^2 \rangle$ (via Eq. 16), and $\Omega_{wcc}/\langle r^2 \rangle$ (via Eq. 11), respectively.

**Table 3. Predictions for magnetic octupole moments for isotopes with valence protons in subshell  $2p_{3/2}$**

Predictions for isotopes with a (bare) valence proton in subshell  $2p_{3/2}$ . The respective spin/parity ( $I^\pi$ ) is also shown (from Ref. [66]). All values are in  $\mu_N$  units. The various  $\Omega$  terms are calculated using Eqs. 3, 7, 9, 10, 11, 16 and 17, similarly to Tables 1 and 2.

**Table 4. Predictions for magnetic octupole moments for isotopes with valence protons in subshell  $1g_{9/2}$**

Predictions for isotopes with a (bare) valence proton in subshell  $1g_{9/2}$ . The respective spin/parity ( $I^\pi$ ) is also shown (from Ref. [66]). All values are in  $\mu_N$  units. The various  $\Omega$  terms are calculated using Eqs. 3, 7, 9, 10, 11, 16 and 17, similarly to Tables 1 and 2.

**Table 5. Predictions for magnetic octupole moments for isotopes with valence neutrons in subshell  $1g_{9/2}$**

Collective model predictions (strong and weak coupling) for isotopes with a (bare) valence neutron in subshell  $1g_{9/2}$ . The respective spin/parity ( $I^\pi$ ) is also shown (from Ref. [66]). All values are in  $\mu_N$  units.

Table 1

Comparison between experimental (*exp*) and theoretical (single-particle (*s.p.*) and collective strong (*scc*) and weak (*wcc*) coupling) values of magnetic octupole moments for odd-neutron nuclei.

Isotope	$I^\pi$	Shell assign.	Experimental	Ref.	s.p. model	Collective model				
			$\Omega_{exp}/\langle r^2 \rangle$		$\Omega_{sp}/\langle r^2 \rangle$	Strong coupling		Weak coupling		
Equations used:					(3)	(9)	(7) (10)	(17)	(16)	(11)
$^{83}\text{Kr}$	$\frac{9}{2}^+$	$g_{9/2}$	-0.87(29)	[15]	-2.087 /-1.461	-0.361	-0.719 /-0.535	-1.483 /-1.038	-0.088	-1.571 /-1.126
$^{131}\text{Xe}$	$\frac{3}{2}^+$	$d_{3/2}$	+0.17(4)	[16]	+0.164 /+0.115	-0.343	+0.079 /+0.052	+0.101 /+0.071	-0.056	+0.045 /+0.014
$^{137}\text{Ba}^+$	$\frac{3}{2}^+$	$d_{3/2}$	+0.1742(19) <sup>(a)</sup>	[17]	+0.164 /+0.115	-0.341	+0.079 /+0.053	+0.099 /+0.070	-0.058	+0.042 /+0.012
			+0.1740(18)	[17]						
			+0.171(13)	[17]						
			-0.1681(18) <sup>(b)</sup>	[18]						
			+0.217(4)	[19]						
$^{155}\text{Gd}$	$\frac{3}{2}^-$	$p_{3/2}$	-5.1(1.9)	[20]	-1.148 /-0.803	-0.344	-0.633 /-0.446	-0.592 /-0.414	-0.071	-0.663 /-0.486
$^{173}\text{Yb}$	$\frac{5}{2}^-$	$f_{5/2}$	-101(6)	[21]	+0.547	-0.337	+0.025	-0.056	-0.145	-0.201
			+20(47) <sup>(a)</sup>	[22]	+0.383		+0.005	-0.039		-0.184
$^{201}\text{Hg}$	$\frac{3}{2}^-$	$p_{3/2}$	-0.346(35)	[23]	-1.148 /-0.803	-0.332	-0.633 /-0.446	-0.329 /-0.230	-0.101	-0.430 /-0.332
$^{207}\text{Po}$	$\frac{5}{2}^-$	$f_{5/2}$	+0.287(26)	[24]	+0.547 /+0.383	-0.338	+0.025 /+0.005	-0.433 /-0.303	-0.236	-0.669 /-0.539

Table 2

Comparison between experimental (*exp*) and theoretical (single-particle (*s.p.*) and collective strong (*scc*) and weak (*wcc*) coupling) values of magnetic octupole moments for odd-proton nuclei.

Isotope	$I^\pi$	Shell assign.	Experimental	Ref.	s.p. model	Collective model				
						$\Omega_{exp}/\langle r^2 \rangle$	Strong coupling		Weak coupling	
			$\Omega_{sp}/\langle r^2 \rangle$		$\Omega_o/\langle r^2 \rangle$	$\Omega_{scc}/\langle r^2 \rangle$	$\Omega_p/\langle r^2 \rangle$	$\Omega_c/\langle r^2 \rangle$	$\Omega_{wcc}/\langle r^2 \rangle$	
Equations used:					(3)	(9)	(7) (10)	(17)	(16)	(11)
$^{35}\text{Cl}$	$\frac{3}{2}^+$	$d_{3/2}$	$-0.1607(26)^{(a)}$	[6]	$-0.068$ /+0.021	$-0.405$	$-0.048$ /-0.000	$-0.051$ /+0.016	$-0.043$	$-0.094$ /-0.027
			$-0.1607^{(b)}$	[7]						
			$-0.1385^{(b)}$	[7]						
			$-0.1632(27)$	[8]						
$^{37}\text{Cl}$	$\frac{3}{2}^+$	$d_{3/2}$	$-0.1202(25)^{(a)}$	[6]	$-0.068$ /+0.021	$-0.383$	$-0.048$ /+0.000	$-0.051$ /+0.016	$-0.040$	$-0.091$ /-0.024
			$-0.122(26)$	[8]						
$^{45}\text{Sc}$	$\frac{7}{2}^-$	$f_{7/2}$	$+12(6)$	[28]	$+3.794$ /+3.055	$-0.389$	$+0.722$ /+0.566	$+2.430$ /+1.957	$-0.084$	$+2.347$ /+1.874
$^{69}\text{Ga}$	$\frac{3}{2}^-$	$p_{3/2}$	$+0.745(27)^{(a)}$	[6]	$+1.676$ /+1.173	$-0.374$	$+0.899$ /+0.626	$+1.207$ /+0.845	$-0.045$	$+1.162$ /+0.800
			$+0.58(11)$	[25]						
$^{71}\text{Ga}$	$\frac{3}{2}^-$	$p_{3/2}$	$+0.960(27)^{(a)}$	[6]	$+1.676$ /+1.173	$-0.364$	$+0.899$ /+0.627	$+1.217$ /+0.852	$-0.043$	$+1.174$ /+0.809
			$+0.78(11)$	[25]						
$^{79}\text{Br}$	$\frac{3}{2}^-$	$p_{3/2}$	$+0.461^{(a),(b)}$	[7]	$+1.676$ /+1.173	$-0.369$	$+0.899$ /+0.626	$+1.183$ /+0.828	$-0.047$	$+1.137$ /+0.782
			$+0.611^{(b)}$	[7]						
			$+0.576^{(b)}$	[9]						
$^{81}\text{Br}$	$\frac{3}{2}^-$	$p_{3/2}$	$+0.630^{(b)}$	[9]	$+1.676$ /+1.173	$-0.360$	$+0.900$ /+0.627	$+1.194$ /+0.836	$-0.044$	$+1.149$ /+0.791
$^{87}\text{Rb}$	$\frac{3}{2}^-$	$p_{3/2}$	$-2.7(18)$	[10]	$+1.676$ /+1.173	$-0.354$	$+0.900$ /+0.627	$+1.186$ /+0.830	$-0.044$	$+1.142$ /+0.786
$^{113}\text{In}$	$\frac{9}{2}^+$	$g_{9/2}$	$+2.25(6)$	[11]	$+4.684$ /+3.933	$-0.361$	$+1.270$ /+1.049	$+2.971$ /+2.495	$-0.111$	$+2.861$ /+2.385
$^{115}\text{In}$	$\frac{9}{2}^+$	$g_{9/2}$	$+1.84(4)^{(a)}$	[6]	$+4.684$ /+3.933	$-0.355$	$+1.271$ /+1.051	$+3.011$ /+2.528	$-0.106$	$+2.905$ /+2.422
			$+2.18(5)$	[11]						
$^{127}\text{I}$	$\frac{5}{2}^+$	$d_{5/2}$	$+0.66(17)^{(a)}$	[6]	$+2.823$ /+2.148	$-0.348$	$+0.295$ /+0.214	$+0.646$ /+0.492	$-0.104$	$+0.542$ /+0.387
			$+1^{(b)}$	[26]						
			$+0.959^{(b)}$	[7]						
			$+0.604^{(b)}$	[7]						
$^{133}\text{Cs}$	$\frac{7}{2}^+$	$g_{7/2}$	$+2.9(4)$	[12]	$+0.094$ /+0.611	$-0.345$	$-0.053$ /+0.057	$+0.042$ /+0.271	$-0.115$	$-0.073$ /+0.156
$^{197}\text{Au}$	$\frac{3}{2}^+$	$d_{3/2}$	$+0.0265(19)^{(a)}$	[13]	$-0.068$ /+0.021	$-0.334$	$-0.046$ /+0.002	$-0.020$ /+0.006	$-0.101$	$-0.121$ /-0.095
			$+0.35^{(b)}$	[13]						
			$+0.16(16)$	[13]						
$^{209}\text{Bi}$	$\frac{9}{2}^-$	$h_{9/2}$	$+1.43(8)^{(a)}$	[14]	$+0.415$ /+1.113	$-0.331$	$+0.025$ /+0.230	$+0.092$ /+0.246	$-0.216$	$-0.124$ /+0.031
			$+1.12^{(b)}$	[27]						
			$+1.61(21)$	[29]						

Table 3: Collective model predictions (strong and weak coupling) for isotopes with a (bare) valence proton in subshell  $2p_{3/2}$ . All values are quoted in  $\mu_N$  units. See explanation of tables for more details.

Isotope	$I^\pi$	Collective Model				
		<i>Strong coupling</i>		<i>Weak coupling</i>		
		$\frac{\Omega_o}{\langle r^2 \rangle}$	$\frac{\Omega_{scc}}{\langle r^2 \rangle}$	$\frac{\Omega_p}{\langle r^2 \rangle}$	$\frac{\Omega_c}{\langle r^2 \rangle}$	$\frac{\Omega_{wcc}}{\langle r^2 \rangle}$
$^{55}\text{Cu}$	$\frac{3}{2}^-$	-0.439	+0.897	+1.158	-0.058	+1.100
$^{57}\text{Cu}$	$\frac{3}{2}^-$	-0.424	+0.898	+1.173	-0.055	+1.119
$^{59}\text{Cu}$	$\frac{3}{2}^-$	-0.410	+0.898	+1.187	-0.051	+1.136
$^{61}\text{Cu}$	$\frac{3}{2}^-$	-0.396	+0.899	+1.200	-0.048	+1.151
$^{63}\text{Cu}$	$\frac{3}{2}^-$	-0.384	+0.899	+1.211	-0.046	+1.166
$^{65}\text{Cu}$	$\frac{3}{2}^-$	-0.372	+0.899	+1.222	-0.043	+1.178
$^{67}\text{Cu}$	$\frac{3}{2}^-$	-0.361	+0.900	+1.231	-0.041	+1.190
$^{69}\text{Cu}$	$\frac{3}{2}^-$	-0.350	+0.900	+1.240	-0.039	+1.201
$^{71}\text{Cu}$	$\frac{3}{2}^-$	-0.340	+0.900	+1.248	-0.037	+1.211
$^{73}\text{Cu}$	$\frac{3}{2}^-$	-0.331	+0.900	+1.256	-0.036	+1.220
$^{59}\text{Ga}$	$\frac{3}{2}^-$	-0.438	+0.897	+1.140	-0.060	+1.079
$^{61}\text{Ga}$	$\frac{3}{2}^-$	-0.423	+0.898	+1.156	-0.056	+1.099
$^{63}\text{Ga}$	$\frac{3}{2}^-$	-0.410	+0.898	+1.170	-0.053	+1.117
$^{65}\text{Ga}$	$\frac{3}{2}^-$	-0.397	+0.899	+1.183	-0.050	+1.133
$^{67}\text{Ga}$	$\frac{3}{2}^-$	-0.385	+0.899	+1.195	-0.047	+1.148
$^{73m}\text{Ga}$	$\frac{3}{2}^-$	-0.354	+0.900	+1.226	-0.041	+1.185
$^{75}\text{Ga}$	$\frac{3}{2}^-$	-0.344	+0.900	+1.235	-0.039	+1.196
$^{77}\text{Ga}$	$\frac{3}{2}^-$	-0.335	+0.900	+1.243	-0.037	+1.206
$^{79}\text{Ga}$	$\frac{3}{2}^-$	-0.327	+0.901	+1.250	-0.036	+1.215
$^{61}\text{As}$	$\frac{3}{2}^-$	-0.451	+0.897	+1.101	-0.066	+1.034
$^{63}\text{As}$	$\frac{3}{2}^-$	-0.436	+0.897	+1.119	-0.062	+1.057
$^{65}\text{As}$	$\frac{3}{2}^-$	-0.423	+0.898	+1.136	-0.058	+1.078
$^{73}\text{As}$	$\frac{3}{2}^-$	-0.377	+0.899	+1.190	-0.047	+1.143
$^{75}\text{As}$	$\frac{3}{2}^-$	-0.367	+0.899	+1.201	-0.045	+1.156
$^{77}\text{As}$	$\frac{3}{2}^-$	-0.357	+0.900	+1.211	-0.043	+1.168
$^{79}\text{As}$	$\frac{3}{2}^-$	-0.348	+0.900	+1.220	-0.041	+1.179
$^{81}\text{As}$	$\frac{3}{2}^-$	-0.339	+0.900	+1.228	-0.039	+1.190
$^{87}\text{As}$	$\left(\frac{5}{2}^-, \frac{3}{2}^-\right)$	-0.316	+0.901	+1.251	-0.034	+1.216
$^{75}\text{Br}$	$\frac{3}{2}^-$	-0.389	+0.899	+1.159	-0.051	+1.108
$^{77}\text{Br}$	$\frac{3}{2}^-$	-0.379	+0.899	+1.172	-0.049	+1.123
$^{83}\text{Br}$	$\frac{3}{2}^-$	-0.351	+0.900	+1.204	-0.042	+1.161
$^{85}\text{Br}$	$\frac{3}{2}^-$	-0.343	+0.900	+1.213	-0.041	+1.172
$^{89}\text{Br}$	$\left(\frac{3}{2}^-, \frac{5}{2}^-\right)$	-0.328	+0.901	+1.229	-0.037	+1.192
$^{73}\text{Rb}$	$\frac{3}{2}^-$	-0.422	+0.898	+1.092	-0.063	+1.029
$^{75}\text{Rb}$	$\frac{3}{2}^-$	-0.411	+0.898	+1.109	-0.060	+1.049
$^{77}\text{Rb}$	$\frac{3}{2}^-$	-0.400	+0.898	+1.125	-0.056	+1.068
$^{81}\text{Rb}$	$\frac{3}{2}^-$	-0.381	+0.899	+1.152	-0.051	+1.101

Continued on next page

Continued from previous page						
$^{89}\text{Rb}$	$\frac{3}{2}^-$	-0.346	+0.900	+1.196	-0.043	+1.153
$^{91}\text{Rb}$	$\frac{3}{2}^-$	-0.339	+0.900	+1.205	-0.041	+1.164
$^{97m}\text{Rb}$	$\left(\frac{1}{2}, \frac{3}{2}\right)^-$	-0.318	+0.901	+1.229	-0.036	+1.192
$^{83m}\text{Y}$	$\left(\frac{3}{2}^-\right)$	-0.391	+0.899	+1.116	-0.056	+1.060
$^{109}\text{Nb}$	$\frac{3}{2}^-$	-0.313	+0.901	+1.211	-0.037	+1.173
$^{111}\text{Nb}$	$\frac{3}{2}^-$	-0.308	+0.901	+1.218	-0.036	+1.182
$^{113}\text{Nb}$	$\frac{3}{2}^-$	-0.302	+0.901	+1.225	-0.035	+1.190
$^{115}\text{Nb}$	$\frac{3}{2}^-$	-0.297	+0.901	+1.231	-0.034	+1.198
$^{105}\text{Tc}$	$\left(\frac{3}{2}^-\right)$	-0.341	+0.900	+1.157	-0.045	+1.111
$^{107}\text{Tc}$	$\left(\frac{3}{2}^-\right)$	-0.335	+0.900	+1.167	-0.044	+1.123



Table 4: Collective model predictions (strong and weak coupling) for isotopes with a (bare) valence proton in subshell  $2p_{3/2}$ . All values are quoted in  $\mu_N$  units. See explanation of tables for more details.

Isotope	$I^\pi$	Collective Model				
		<i>Strong coupling</i>		<i>Weak coupling</i>		
		$\frac{\Omega_p}{\langle r^2 \rangle}$	$\frac{\Omega_{acc}}{\langle r^2 \rangle}$	$\frac{\Omega_p}{\langle r^2 \rangle}$	$\frac{\Omega_c}{\langle r^2 \rangle}$	$\frac{\Omega_{wcc}}{\langle r^2 \rangle}$
$73^m\text{As}$	$\frac{9}{2}^+$	-0.377	+1.265	+3.343	-0.090	+3.252
$75^m\text{As}$	$\frac{9}{2}^+$	-0.367	+1.268	+3.372	-0.086	+3.286
$77^m\text{As}$	$\frac{9}{2}^+$	-0.357	+1.271	+3.400	-0.082	+3.318
$79^m\text{As}$	$\left(\frac{9}{2}\right)^+$	-0.348	+1.273	+3.425	-0.078	+3.347
$77^m\text{Br}$	$\frac{9}{2}^+$	-0.379	+1.264	+3.293	-0.094	+3.199
$79^m\text{Br}$	$\frac{9}{2}^+$	-0.369	+1.267	+3.324	-0.090	+3.235
$81^m\text{Br}$	$\frac{9}{2}^+$	-0.360	+1.270	+3.353	-0.086	+3.268
$73^m\text{Rb}$	$\frac{9}{2}^+$	-0.422	+1.252	+3.072	-0.122	+2.950
$81^m\text{Rb}$	$\frac{9}{2}^+$	-0.381	+1.264	+3.238	-0.098	+3.140
$83^m\text{Rb}$	$\frac{9}{2}^+$	-0.371	+1.267	+3.272	-0.094	+3.178
$85^m\text{Rb}$	$\frac{9}{2}^+$	-0.363	+1.269	+3.303	-0.090	+3.213
$95^m\text{Rb}$	$\frac{9}{2}^+$	-0.324	+1.280	+3.429	-0.073	+3.356
$83\text{Y}$	$\left(\frac{9}{2}\right)^+$	-0.391	+1.261	+3.140	-0.108	+3.032
$85^m\text{Y}$	$\left(\frac{9}{2}\right)^+$	-0.382	+1.263	+3.179	-0.103	+3.076
$87^m\text{Y}$	$\frac{9}{2}^+$	-0.373	+1.266	+3.214	-0.098	+3.116
$89^m\text{Y}$	$\frac{9}{2}^+$	-0.365	+1.268	+3.248	-0.094	+3.154
$91^m\text{Y}$	$\frac{9}{2}^+$	-0.357	+1.271	+3.279	-0.090	+3.189
$93^m\text{Y}$	$\frac{9}{2}^+$	-0.349	+1.273	+3.307	-0.086	+3.221
$95^m\text{Y}$	$\frac{9}{2}^+$	-0.342	+1.275	+3.334	-0.083	+3.252
$97^m\text{Y}$	$\frac{9}{2}^+$	-0.335	+1.277	+3.359	-0.079	+3.280
$79\text{Nb}$	$\frac{9}{2}^+$	-0.432	+1.249	+2.863	-0.141	+2.722
$81\text{Nb}$	$\frac{9}{2}^+$	-0.422	+1.252	+2.923	-0.133	+2.790
$83\text{Nb}$	$\frac{9}{2}^+$	-0.412	+1.255	+2.977	-0.126	+2.851
$85\text{Nb}$	$\frac{9}{2}^+$	-0.402	+1.258	+3.026	-0.119	+2.907
$87^m\text{Nb}$	$\left(\frac{9}{2}\right)^+$	-0.393	+1.260	+3.072	-0.113	+2.958
$89\text{Nb}$	$\left(\frac{9}{2}\right)^+$	-0.384	+1.263	+3.113	-0.108	+3.005
$91\text{Nb}$	$\frac{9}{2}^+$	-0.375	+1.265	+3.152	-0.103	+3.049
$93\text{Nb}$	$\frac{9}{2}^+$	-0.367	+1.268	+3.188	-0.098	+3.089
$95\text{Nb}$	$\frac{9}{2}^+$	-0.360	+1.270	+3.221	-0.094	+3.127
$97\text{Nb}$	$\frac{9}{2}^+$	-0.352	+1.272	+3.252	-0.090	+3.161
$99\text{Nb}$	$\frac{9}{2}^+$	-0.345	+1.274	+3.280	-0.087	+3.194
$87\text{Tc}$	$\frac{9}{2}^+$	-0.412	+1.255	+2.895	-0.132	+2.763
$89\text{Tc}$	$\left(\frac{9}{2}\right)^+$	-0.403	+1.257	+2.948	-0.125	+2.823
$91\text{Tc}$	$\left(\frac{9}{2}\right)^+$	-0.394	+1.260	+2.997	-0.119	+2.878
$93\text{Tc}$	$\frac{9}{2}^+$	-0.385	+1.263	+3.042	-0.113	+2.929
$95\text{Tc}$	$\frac{9}{2}^+$	-0.377	+1.265	+3.083	-0.108	+2.975
$97\text{Tc}$	$\frac{9}{2}^+$	-0.369	+1.267	+3.122	-0.103	+3.019

Continued on next page

Continued from previous page

$^{99}\text{Tc}$	$\frac{9^+}{2}$	-0.362	+1.269	+3.157	-0.099	+3.059
$^{101}\text{Tc}$	$\frac{9^+}{2}$	-0.355	+1.271	+3.191	-0.095	+3.096
$^{89}\text{Rh}$	$\frac{9^+}{2}$	-0.421	+1.252	+2.741	-0.146	+2.595
$^{91}\text{Rh}$	$\left(\frac{9^+}{2}\right)$	-0.412	+1.255	+2.804	-0.138	+2.666
$^{93}\text{Rh}$	$\frac{9^+}{2}$	-0.403	+1.257	+2.862	-0.131	+2.730
$^{95}\text{Rh}$	$\left(\frac{9^+}{2}\right)^+$	-0.395	+1.260	+2.915	-0.125	+2.790
$^{97}\text{Rh}$	$\frac{9^+}{2}$	-0.387	+1.262	+2.963	-0.119	+2.844
$^{99m}\text{Rh}$	$\frac{9^+}{2}$	-0.379	+1.264	+3.008	-0.113	+2.895
$^{101m}\text{Rh}$	$\frac{9^+}{2}$	-0.371	+1.267	+3.050	-0.108	+2.941
$^{93}\text{Ag}$	$\frac{9^+}{2}$	-0.421	+1.252	+2.635	-0.154	+2.481
$^{95}\text{Ag}$	$\left(\frac{9^+}{2}\right)$	-0.412	+1.255	+2.704	-0.146	+2.558
$^{97}\text{Ag}$	$\left(\frac{9^+}{2}\right)^+$	-0.404	+1.257	+2.766	-0.138	+2.628
$^{99}\text{Ag}$	$\left(\frac{9^+}{2}\right)^+$	-0.396	+1.259	+2.824	-0.132	+2.692
$^{101}\text{Ag}$	$\frac{9^+}{2}$	-0.388	+1.262	+2.877	-0.125	+2.751
$^{125}\text{Ag}$	$\left(\frac{9^+}{2}\right)$	-0.313	+1.284	+3.288	-0.078	+3.209
$^{127}\text{Ag}$	$\left(\frac{9^+}{2}\right)$	-0.308	+1.285	+3.310	-0.076	+3.234
$^{129}\text{Ag}$	$\frac{9^+}{2}$	-0.304	+1.287	+3.332	-0.073	+3.258
$^{131}\text{Ag}$	$\frac{9^+}{2}$	-0.299	+1.288	+3.352	-0.071	+3.281
$^{133}\text{Ag}$	$\frac{9^+}{2}$	-0.294	+1.289	+3.371	-0.069	+3.302
$^{97}\text{In}$	$\frac{9^+}{2}$	-0.421	+1.252	+2.518	-0.163	+2.355
$^{99}\text{In}$	$\frac{9^+}{2}$	-0.412	+1.255	+2.593	-0.154	+2.438
$^{101}\text{In}$	$\left(\frac{9^+}{2}\right)$	-0.404	+1.257	+2.661	-0.146	+2.515
$^{103}\text{In}$	$\left(\frac{9^+}{2}\right)$	-0.396	+1.259	+2.724	-0.139	+2.585
$^{105}\text{In}$	$\frac{9^+}{2}$	-0.389	+1.261	+2.781	-0.132	+2.649
$^{107}\text{In}$	$\frac{9^+}{2}$	-0.382	+1.264	+2.834	-0.126	+2.708
$^{109}\text{In}$	$\frac{9^+}{2}$	-0.375	+1.266	+2.883	-0.121	+2.763
$^{111}\text{In}$	$\frac{9^+}{2}$	-0.368	+1.268	+2.929	-0.115	+2.814
$^{117}\text{In}$	$\frac{9^+}{2}$	-0.349	+1.273	+3.048	-0.102	+2.946
$^{119}\text{In}$	$\frac{9^+}{2}$	-0.343	+1.275	+3.083	-0.098	+2.985
$^{121}\text{In}$	$\frac{9^+}{2}$	-0.337	+1.277	+3.115	-0.095	+3.021
$^{123}\text{In}$	$\frac{9^+}{2}$	-0.332	+1.278	+3.146	-0.091	+3.055
$^{125}\text{In}$	$\frac{9^+}{2}$	-0.327	+1.280	+3.175	-0.088	+3.087
$^{127}\text{In}$	$\frac{9^+}{2}$	-0.321	+1.281	+3.202	-0.085	+3.117
$^{129}\text{In}$	$\frac{9^+}{2}$	-0.316	+1.283	+3.228	-0.082	+3.146
$^{131}\text{In}$	$\frac{9^+}{2}$	-0.312	+1.284	+3.252	-0.080	+3.173
$^{133}\text{In}$	$\left(\frac{9^+}{2}\right)$	-0.307	+1.286	+3.276	-0.077	+3.198
$^{135}\text{In}$	$\frac{9^+}{2}$	-0.302	+1.287	+3.298	-0.075	+3.223
$^{137}\text{In}$	$\frac{9^+}{2}$	-0.298	+1.288	+3.319	-0.073	+3.246

Table 5: Collective model predictions (strong and weak coupling) for isotopes with a (bare) valence neutron in subshell  $1g_{9/2}$ . All values are quoted in  $\mu_N$  units. See explanation of tables for more details.

Isotope	$I^\pi$	Collective Model				
		<i>Strong coupling</i>		<i>Weak coupling</i>		
		$\frac{\Omega_o}{\langle r^2 \rangle}$	$\frac{\Omega_{scc}}{\langle r^2 \rangle}$	$\frac{\Omega_p}{\langle r^2 \rangle}$	$\frac{\Omega_c}{\langle r^2 \rangle}$	$\frac{\Omega_{wcc}}{\langle r^2 \rangle}$
$^{59m}\text{Cr}$	$\left(\frac{9}{2}^+\right)$	-0.339	-0.712	-1.588	-0.068	-1.656
$^{61m}\text{Fe}$	$\frac{9}{2}^+$	-0.355	-0.717	-1.564	-0.074	-1.639
$^{65m}\text{Fe}$	$\left(\frac{9}{2}^+\right)$	-0.333	-0.711	-1.584	-0.067	-1.651
$^{75}\text{Fe}$	$\frac{9}{2}^+$	-0.289	-0.698	-1.622	-0.054	-1.675
$^{67m}\text{Ni}$	$\frac{9}{2}^+$	-0.348	-0.715	-1.559	-0.074	-1.633
$^{69}\text{Ni}$	$\left(\frac{9}{2}^+\right)$	-0.338	-0.712	-1.569	-0.070	-1.639
$^{71}\text{Ni}$	$\left(\frac{9}{2}^+\right)$	-0.329	-0.709	-1.578	-0.067	-1.645
$^{73}\text{Ni}$	$\left(\frac{9}{2}^+\right)$	-0.320	-0.707	-1.587	-0.064	-1.651
$^{75}\text{Ni}$	$\frac{9}{2}^+$	-0.311	-0.704	-1.595	-0.061	-1.656
$^{77}\text{Ni}$	$\frac{9}{2}^+$	-0.303	-0.702	-1.602	-0.059	-1.661
$^{69m}\text{Zn}$	$\frac{9}{2}^+$	-0.362	-0.719	-1.531	-0.081	-1.612
$^{71m}\text{Zn}$	$\frac{9}{2}^+$	-0.352	-0.716	-1.543	-0.077	-1.620
$^{79}\text{Zn}$	$\frac{9}{2}^+$	-0.316	-0.706	-1.580	-0.064	-1.644
$^{71m}\text{Ge}$	$\frac{9}{2}^+$	-0.376	-0.723	-1.500	-0.088	-1.588
$^{73}\text{Ge}$	$\frac{9}{2}^+$	-0.365	-0.720	-1.513	-0.084	-1.597
$^{81}\text{Ge}$	$\frac{9}{2}^+$	-0.329	-0.710	-1.555	-0.070	-1.625
$^{73}\text{Se}$	$\frac{9}{2}^+$	-0.388	-0.727	-1.464	-0.097	-1.561
$^{83}\text{Se}$	$\frac{9}{2}^+$	-0.341	-0.713	-1.527	-0.077	-1.604
$^{73m}\text{Kr}$	$\left(\frac{9}{2}^+\right)$	-0.411	-0.734	-1.404	-0.113	-1.516
$^{85}\text{Kr}$	$\frac{9}{2}^+$	-0.353	-0.717	-1.496	-0.084	-1.579
$^{85}\text{Sr}$	$\frac{9}{2}^+$	-0.372	-0.722	-1.445	-0.096	-1.541
$^{87}\text{Sr}$	$\frac{9}{2}^+$	-0.364	-0.720	-1.460	-0.092	-1.551
$^{87}\text{Zr}$	$\frac{9}{2}^+$	-0.383	-0.725	-1.402	-0.105	-1.507
$^{89}\text{Zr}$	$\frac{9}{2}^+$	-0.374	-0.723	-1.419	-0.100	-1.519
$^{89}\text{Mo}$	$\left(\frac{9}{2}^+\right)$	-0.393	-0.728	-1.352	-0.116	-1.468
$^{91}\text{Mo}$	$\frac{9}{2}^+$	-0.385	-0.726	-1.372	-0.110	-1.482
$^{89}\text{Ru}$	$\left(\frac{9}{2}^+\right)$	-0.412	-0.734	-1.270	-0.135	-1.405
$^{91}\text{Ru}$	$\left(\frac{9}{2}^+\right)$	-0.403	-0.731	-1.295	-0.128	-1.423
$^{93}\text{Ru}$	$\left(\frac{9}{2}^+\right)$	-0.394	-0.729	-1.317	-0.122	-1.439
$^{93}\text{Pd}$	$\left(\frac{9}{2}^+\right)$	-0.412	-0.734	-1.228	-0.142	-1.370
$^{95}\text{Pd}$	$\frac{9}{2}^+$	-0.403	-0.731	-1.254	-0.135	-1.389
$^{95}\text{Cd}$	$\frac{9}{2}^+$	-0.421	-0.737	-1.149	-0.158	-1.307
$^{97}\text{Cd}$	$\left(\frac{9}{2}^+\right)$	-0.412	-0.734	-1.181	-0.150	-1.331
$^{99}\text{Sn}$	$\frac{9}{2}^+$	-0.421	-0.737	-1.093	-0.168	-1.261